Acta Crystallographica Section D
Biological Crystallography
ISSN 0907-4449

Structure of DsbC from *Haemophilus influenzae*

Man Zhang,[a] Arthur F. Monzingo,[a] Laura Segatori,[b] George Georgiou[b] and Jon D. Robertus[a]*

[a]Institute for Cellular and Molecular Biology, Department of Chemistry and Biochemistry, 1 University Station, University of Texas at Austin, Austin, TX 78712, USA, and [b]Department of Chemical Engineering, 1 University Station, University of Texas at Austin, Austin, TX 78712, USA

Correspondence e-mail: jrobertus@mail.utexas.edu

Received 27 April 2004
Accepted 15 June 2004

PDB Reference: DsbC, 1t3b, r1t3bsf.

Bacterial DsbC proteins are involved in rearranging or reducing mismatched disulfide bonds folding within the periplasm. The X-ray structure of the enzyme from *Haemophilus influenzae* has been solved and compared with the known structure of the *Escherichia coli* protein. The proteins act as V-shaped dimers with a large cleft to accommodate substrate proteins. The dimers are anchored by a small N-terminal domain, but have a flexible linker region which allows the larger C-terminal domain, with its reactive sulfhydryls, to clamp down on substrates. The overall folds are very similar, but the comparison shows a wider range of hinge motions than previously thought. The crystal packing of the *H. influenzae* protein allows the movement of the N-terminal domain with respect to the C-terminal domain through motions in the flexible hinge, generating high thermal parameters and unusually high anisotropy in the crystallographic data.

1. Introduction

Disulfide bonds are important for protein stability, especially for secreted proteins exposed to the rigors of the extracellular environment. In Gram-negative bacteria, a family of proteins has been identified that play important roles in protein disulfide oxidation and isomerization; this family is referred to collectively as the Dsb (disulfide-bond) proteins (Bardwell *et al.*, 1991). There is little primary sequence similarity among the Dsb proteins except that they all share an active-site –C*XX*C– sequence, which is characteristic of redox proteins with a thioredoxin fold (Raina & Missiakas, 1997). X-ray structural analysis has confirmed that the thioredoxin fold exists in DsbA (Martin *et al.*, 1993), DsbC (McCarthy *et al.*, 2000), DsbDγ (Kim *et al.*, 2003) and DsbE (Edeling *et al.*, 2002).

Formation of correct disulfide bonds in newly synthesized proteins is generally a multistep process. Protein thiols are initially oxidized to disulfides in Gram-negative bacteria by DsbA. A mixed disulfide bond is formed between the target-protein thiol and an active-site thiol of DsbA. The disulfide is then transferred to the target protein to form an internal disulfide, leaving the active-site pair of DsbA reduced (Bardwell *et al.*, 1993). Subsequently, the reduced DsbA is oxidized by the inner membrane protein DsbB (Guilhot *et al.*, 1995; Kishigami *et al.*, 1995). Under aerobic conditions, the ultimate oxidizing equivalents required by the DsbB–DsbA pathway come from molecular oxygen *via* ubiquinone and cytochrome *bo*/*bd* oxidase (Bader *et al.*, 1999). Under anaerobic conditions, DsbB transfers its electrons to menaquinone and on to either fumarate reductase or nitrate reductase (Bader *et al.*, 1999).

In proteins with multiple thiols, it is possible that the initially formed disulfides are incorrectly matched, producing a non-native protein fold. A disulfide-isomerization pathway must then rearrange the misfolded disulfide bonds, facilitating the correct pairing. DsbC participates in this refolding, as indicated by the observation that the correct folding of multiple disulfide proteins was impaired more than the correct folding of single disulfide proteins in a dsbC null mutant *in vivo* (Rietsch *et al.*, 1996). Previously, *in vitro* assays had shown the ability of DsbC to act as a protein disulfide isomerase (Zapun *et al.*, 1995).

DsbC was found to exist predominantly in the reduced form *in vivo* (Rietsch *et al.*, 1997), which is consistent with its role as an isomerase. The following mechanism of isomerization has been proposed. Cys98 of DsbC attacks an incorrect disulfide bond in the target protein to form a mixed disulfide. The mixed-disulfide complex is then resolved in one of two ways. In one case, an attack from another cysteine on the substrate protein forms a more stable interprotein disulfide bond and releases DsbC in the reduced form. Another possibility is an attack on the mixed disulfide by Cys101 of DsbC, resulting in the release of oxidized DsbC and the reduced target protein (Zapun *et al.*, 1995). In the latter case, the reduced substrate protein will have a second chance of being oxidized by DsbA in order to reach its native conformation. The oxidized DsbC will be reduced by the inner membrane protein DsbD. The reducing electrons are proposed to flow from NADPH to thioredoxin, to DsbD and finally to DsbC through a thiol–disulfide exchange reaction between the α-domain of DsbD and DsbC (Collet *et al.*, 2002).

In addition to DsbC, DsbG can also serve as a protein disulfide isomerase, but has different substrate specificity (Bessette *et al.*, 1999). Like DsbC, DsbG relies on DsbD to be maintained in the reduced form.

Escherichia coli makes very few proteins with disulfide bonds and these have only simple bond patterns. They lack PDI, the major disulfide isomerase of eukaryotes. In general, bacteria have limited protein disulfide-isomerase activity and consequently many recombinant eukaryotic proteins with multiple disulfide bonds have difficulty being folded correctly in *E. coli*. Overexpression of DsbC has been shown to improve the expression and folding of some disulfide-bond-containing recombinant proteins in *E. coli* (Maskos *et al.*, 2003; Kurokawa *et al.*, 2003). For example, the yield of human tissue-type plasminogen activator (t-PA), with 17 disulfide bonds, was increased over 100-fold when DsbC was overexpressed in *E. coli* (Qiu *et al.*, 1998).

DsbC is a 21 kDa periplasmic protein and forms a stable homodimer (Zapun *et al.*, 1995) which is required for isomerase activity (Bader *et al.*, 2001). DsbC was also reported to possess protein-chaperone activity (Chen *et al.*, 1999). The crystal structure of *E. coli* DsbC shows that the protein exists as a V-shaped homodimer and that dimerization is facilitated through the N-terminal domain (residues 1–61). There is a large hydrophobic cleft between the C-terminal domains of the two monomers, which is proposed to be the polypeptide substrate-binding site (McCarthy *et al.*, 2000; Haebel *et al.*, 2002).

To date, only the *E. coli* DsbC structure has been solved. It is anticipated that the analysis of additional DsbC proteins will improve our understanding of the structure–function relationship of DsbC, including how substrates are recognized and how the protein chaperone and isomerase activity are coordinated. A better understanding of the structure–function relationship of DsbC may also provide guidance in engineering DsbC variants that are more efficient at dealing with passenger proteins and thereby make *E. coli* a better expression system for heterologous proteins. Here, we report the crystal structure of *Haemophilus influenzae* DsbC at a nominal resolution of 3.3 Å.

2. Materials and methods

2.1. Expression and purification of DsbC

The *H. influenzae dsbC* coding region was amplified from expression plasmid pTrc99Ahinf (constructed in the Georgiou laboratory, unpublished work) by the polymerase chain reaction (PCR) using the primers 5′-CGTCTAGATCATGAAGAAAATTTTTACCGCACTTTTG-3′ and 5′-AAGCTCGAGTTGTGCCGTTTCTTC-3′. The PCR product was digested with *Bsp*HI and *Xho*I and ligated into an *Nco*I/*Xho*I-digested pET-28a expression vector (Novagen, Madison, WI, USA); the new plasmid was called pETHinfdsbC. Plasmid construction was verified by automated DNA sequencing. The plasmid pETHinfdsbC contains the coding sequence for *H. influenzae* DsbC fused to a six-histidine tag at its C-terminus. pETHinfdsbC was transformed into *E. coli* cell strain BL21(DE3). Overnight cultures were diluted 100-fold in LB medium (1% tryptone, 1% NaCl and 0.5% yeast extract) with 50 µg ml^{-1} kanamycin at 310 K to mid-log phase ($A_{600} \simeq 0.5$). Protein synthesis was induced by the addition of isopropyl-β-D-thiogalactopyranoside (IPTG) to a final concentration of 0.01 m*M*. These growth conditions were found to maximize the expression of soluble mature protein in the periplasm. After 4 h induction at 303 K, cells were harvested by centrifugation at 6500*g* at 277 K for 10 min.

Soluble periplasmic proteins were released from the cell pellet by osmotic shock. Cells were harvested by centrifugation (500 ml for 15 min at 6500 rev min^{-1}) and the cell pellet was immediately resuspended in 30 m*M* Tris pH 8.5, 0.5 m*M* EDTA, 20% sucrose (100 ml) and gently stirred at room temperature for 10 min. Cells were spun for 15 min at 8500 rev min^{-1}, resuspended in 5 m*M* Tris pH 8.5, 0.5 m*M* EDTA and stirred for 20 min at 277 K. The soluble fraction was separated by centrifugation (30 min at 10 000 rev min^{-1}) and filtered.

His_6-DsbC was purified by immobilized metal-affinity chromatography (IMAC) using a 10 ml Poly Prep Chromatography column (BioRad, Hercules, CA, USA) pre-loaded with nickel and following standard protocols (Novagen, Madison, WI, USA). After loading the periplasmic fraction, the column was stabilized with binding buffer (5 m*M* imida-

zole, 0.5 *M* NaCl, 20 m*M* Tris–HCl pH 7.9) and washed with wash buffer (60 m*M* imidazole, 0.5 *M* NaCl, 20 m*M* Tris–HCl pH 7.9). The His-tagged protein was then eluted with elution buffer (1 *M* imidazole, 0.5 *M* NaCl, 20 m*M* Tris–HCl pH 7.9).

The eluted product was further purified by size-exclusion chromatography using a Superdex200 column (Amersham Pharmacia, Piscataway, NJ, USA) pre-equilibrated in 10 m*M* Tris–HCl pH 7.0. The purity of DsbC revealed by Coomassie Blue-stained SDS gel was over 98%. No reducing agents were added; the protein was therefore in the oxidized form.

2.2. Crystallization

Initial crystallization trials of *H. influenzae* DsbC used protein at 5 mg ml^{-1} in 10 m*M* Tris–HCl pH 7.0. Tests were conducted with commercial screening kits (Hampton Research, Laguna Niguel, CA, USA; Emerald BioStructures, Bainbridge Island, WA, USA) together with a variety of in-house screens. Hanging drops containing equal volumes (2.5 µl) of protein sample and mother liquor were vapor-equilibrated against 400 µl reservoir buffer at both room temperature and 277 K. Crystals were originally obtained from condition No. 41 of the Hampton Research Crystal Screen kit (10% 2-propanol, 20% PEG 4000, 0.1 *M* HEPES pH 7.5). After several rounds of optimization, single crystals of *H. influenzae* DsbC grew within 2–3 d at 277 K from hanging drops over reservoir buffer containing 0.1 *M* sodium phosphate pH 6.5 and 20–24% PEG 4000. In addition to the mixture of reservoir buffer and protein solution, the hanging drop also contained 3–6% glycerol.

Dehydration of *E. coli* DsbC crystals resulted in improved diffraction (McCarthy *et al.*, 2000). However, attempts to dehydrate the *H. influenzae* crystals were unsuccessful, resulting in either no improvement in diffraction or damage to the crystal.

2.3. X-ray data collection and processing

Since the *H. influenzae* DsbC crystals were very fragile and sensitive to changes in the precipitant concentration, they were harvested by slowly adding 5 µl of an artificial mother liquor solution (0.1 *M* sodium phosphate pH 6.5, 20–24% PEG 4000, 50% glycerol) into the 5 µl hanging drop containing crystals. After about 10 s, the best crystal from the drop was picked up in a cryoloop (Hampton Research) and flash-cooled in liquid nitrogen. Frozen crystals diffracted as well as crystals at room temperature.

For this study, diffraction data were collected at the Advanced Light Source beamline 8.2.1 at 90 K. The data were integrated and scaled with *DENZO* and *SCALEPACK* (Otwinowski & Minor, 1997). The diffraction pattern of the data collected from the *H. influenzae* DsbC crystal was significantly anisotropic as indicated by the program *TRUNCATE* (French & Wilson, 1978; Collaborative Computational Project, Number 4, 1994). Reflections were observed to 2.5 Å along the c^* axis, but to only 3.3 Å on the plane perpendicular to the c^* axis. Because of the severe anisotropy, a three-dimensional ellipsoid was defined and merging *R* factors and $I/\sigma(I)$ were calculated in ellipsoidal shells as described previously (Lodowski *et al.*, 2003). Diffraction data were then limited to the outermost shell that still contained significant data and the remaining reflections were scaled with a high-resolution limit of 2.5 Å.

Table 1
Crystallographic data.

Values in parentheses are for the last shell (2.50–2.61 Å).

Resolution (c^*, a^*, b^* directions)† (Å)	2.5, 3.3, 3.3
$R_{\rm merge}$ (%)	4.2 (28.4)
$\langle I/\sigma(I)\rangle$	20.1 (3.4)
Completeness‡ (%)	71.3 (35.7)
Completeness $[I/\sigma(I) > 3]$‡ (%)	55.8 (14.0)
Unique reflections	7826
Redundancy	4.5
No. residues	209
No. atoms	1578
$R_{\rm work}$	0.246 (0.389)
$R_{\rm free}$	0.295 (0.498)
R.m.s. deviations from ideality	
Bonds (Å)	0.008
Angles (°)	1.407

† Because of anisotropy, data beyond these limits were excluded during scaling and refinement. ‡ Completeness was determined using the entire sphere of data and the entire spherical last shell.

2.4. Structure determination and refinement

Because of the high sequence homology (45% identity) with *E. coli* DsbC, molecular replacement was chosen for initial phasing of the *H. influenzae* protein. The position of the C-terminal domain of *H. influenzae* DsbC was determined using the *E. coli* DsbC C-terminal domain (residues 78–211; PDB code 1eej) as the search model in the *EPMR* program (Kissinger *et al.*, 2001). Subsequently, the N-terminal domain was located using the *E. coli* N-terminal domain (residues 1–61) as the model.

The two domains of the molecular-replacement model were refined as rigid bodies using *CNS* (v.1.1; Brünger *et al.*, 1998). Owing to the anisotropy of the data, the initial *B*-factor correction for the reflection data was set as 'anisotropic' in all *CNS* refinement.

The initial $2F_{\rm o} - F_{\rm c}$ electron-density map generated using *CNS* was used to fit the hinge-linker region (residues 62–77) and to thread the *H. influenzae* DsbC sequence into the C-terminal domain and hinge-linker region. No side chains were observed in the N-terminal domain and all of these residues were converted to alanine. Density for residues 52–60 was very poor and these residues were not included in the first model of *H. influenzae* DsbC. Several rounds of refinement using *CNS* and model rebuilding using *O* (Jones *et al.*, 1991) followed. Refinement of atomic coordinates and individual atomic temperature factors was performed both with and without the simulated-annealing protocol. σ_A-weighted $2F_{\rm o} - F_{\rm c}$ and $F_{\rm o} - F_{\rm c}$ maps were used for model rebuilding (Read, 1986). By comparing the maps and the working model, backbone and side-chain atoms were added or moved. The stereochemistry of the final refined model was checked using the program *PROCHECK* (Laskowski *et al.*, 1993). Model

building was performed on a Silicon Graphics Indy computer (Mountain View, CA, USA). Computations were performed on a Gateway Select SB computer (Poway, CA, USA).

3. Results and discussion

3.1. Structure determination

The *H. influenzae* DsbC crystals belong to space group $P4_32_12$. The unit-cell parameters are $a = b = 74.92$, $c = 103.38$ Å. There is one molecule per asymmetric unit (V_M = 3.1 Å^3 Da^{-1}). Crystallographic data are summarized in Table 1.

The diffraction data were extremely anisotropic, as first observed from visual inspection of diffraction images and subsequently confirmed by analysis using the program *TRUNCATE*. Significant data were observed to 2.5 Å resolution in the c^* direction, but to only 3.3 Å in the plane perpendicular to c^*. In order to use as many significant data measurements as possible, an ellipsoid of diffraction data, rather than the usual sphere, was used for scaling and refinement.

The initial molecular-replacement solution determined with *EPMR* using the N- and C-terminal domains of the *E. coli* enzyme had an R factor of 49.4% and a correlation coefficient of 0.465. In the initial $2F_o - F_c$ map, density for the backbone and many side chains was visible in the C-terminal catalytic domain (residues 78–211) and the hinge-linker region (residues 62–77). However, in the N-terminal dimerization domain (residues 1–61) no side chains were visible and the density for residues 52–61 was very poor.

With subsequent rounds of refinement and rebuilding of the protein structure, map quality improved such that several side chains could be fitted in the N-terminal domain and residues 52– 61 could be added to the structure. In the final model, 16 residues in the N-terminal domain have no observed side-chain density and are modeled as alanines. By contrast, only four residues in the C-terminal domain and hinge-linker region have no side-chain density. The probable cause of this observed difference in side-chain definition between the two domains is a greater thermal motion in the N-terminal domain, as discussed below. There is also no observed density for residues 1 and 211 and these are not included in the final model. There are ten bound water molecules in the final model, which has an R_{work} of 24.6% and an R_{free} of 29.5%. A Ramachandran plot has 71.0% of residues in the most favorable region, 25.1% in additionally allowed space and 3.8% in generously allowed space. Five of the seven residues with generously allowed φ/ψ angles are in poorly defined regions of the N-terminal domain. A section of the final electron-density map, indicating the map quality, is shown in Fig. 1.

3.2. Overall structure of *H. influenzae* DsbC

The overall structure of the *H. influenzae* DsbC monomer is very similar to that of *E. coli* DsbC. Both have an N-terminal dimerization domain (residues 2–61 in the *H. influenzae* protein), a C-terminal catalytic domain (residues 78–210) and a hinge-linker region (residues 62–77). The C^α trace of the DsbC monomer is shown in Fig. 2.

As expected from the primary sequence, the thioredoxin fold is conserved in the C-terminal domain of *H. influenzae* DsbC. The thioredoxin domain in *E. coli* DsbC has five β-strands ($\beta7$–$\beta11$) flanked by one α-helix ($\alpha6$) on one side and three helices, $\alpha3$, $\alpha3'$ and $\alpha6$, on the opposite side

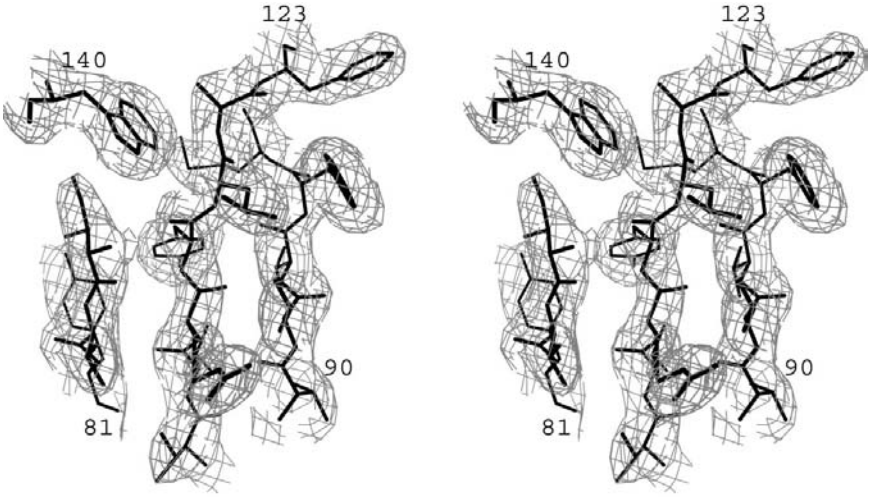

Figure 1
Electron density for the *H. influenzae* DsbC protein. Several labeled segments of the chain are shown superimposed on a $2F_o - F_c$ electron-density map contoured at 1σ. This figure was generated using *BOBSCRIPT* (Esnouf, 1997).

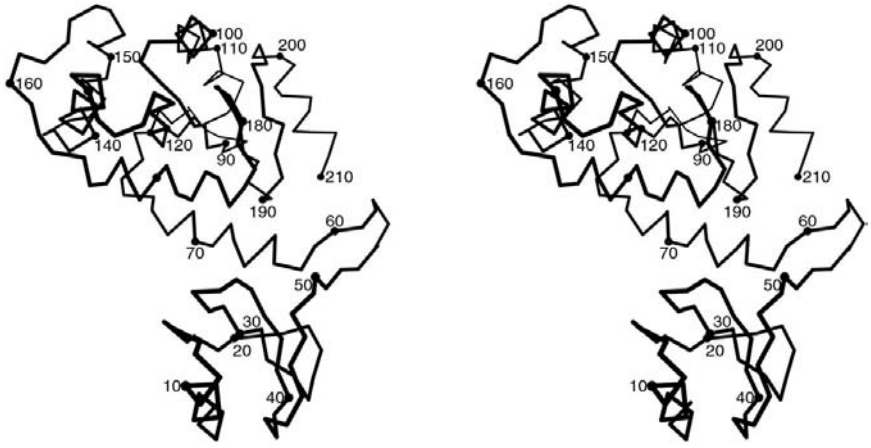

Figure 2
The backbone trace of the *H. influenzae* DsbC protein. In this stereo image, every tenth C^α atom is labeled and shown as a dot. This figure was generated using *BOBSCRIPT* (Esnouf, 1997).

(McCarthy *et al.*, 2000). Similar to *E. coli* DsbC, a helical subdomain containing helices α4 and α5 is inserted into the canonical thioredoxin subdomain. When the C-terminal domain of the *H. influenzae* protein is superimposed with monomer *A* of the *E. coli* dimer, the r.m.s. distance between equivalent C^{α} atoms is 1.6 Å; with monomer *B*, the r.m.s. distance is 1.7 Å. The largest structural difference is in the loop connecting helices α5 and α6. Superposition of the *E. coli* and *H. influenzae* DsbC monomers indicates that the C*XX*C active-site residues are virtually identical. In both cases, Cys98 and Cys101 are found to be oxidized in the crystals to a disulfide at the N-terminus of α3. A Cys101→Ser mutant of the *E. coli* protein has also been observed complexed to the α-domain of DsbD (Haebel *et al.*, 2002). Clearly, the mutated protein cannot form this disulfide. However, the local protein backbone conformation is essentially identical to the disulfide-bonded examples and there is only a slight rotation of the side chains.

Figure 3
Stereoview of the superposition of apo *H. influenzae* DsbC (black) dimer and *E. coli* DsbC mutant (gray) dimer from the DsbC–DsbDα complex. The positions of the two active-site sulfhydryls in each active site are marked by colored spheres. This figure was generated using *BOBSCRIPT* (Esnouf, 1997).

Similar to the C-terminal domains, the tertiary structures of the N-terminal domain and the helical hinge-linker region of the two proteins are virtually identical. When the N-terminal domain and the hinge-linker region of the *H. influenzae* protein and the *E. coli* monomer *A* are superimposed separately, the r.m.s. distances between equivalent C^{α} atoms are 1.5 and 1.1 Å, respectively. The r.m.s. distances with monomer *B* are 1.7 and 0.7 Å, respectively. The largest difference in the N-terminal domain involves the antiparallel β-loop (residues 51–61), which participates in dimerization. With the N-terminal domains superimposed, however, there is a clear difference in the orientation of the C-terminal domains. This is illustrated in Fig. 3, a comparison of the *H. influenzae* DsbC with the *E. coli* protein from the DsbDα complex; a large angular reorientation of the C terminal domains is evident. A superposition with the *E. coli* apoprotein shows that structure is intermediate between these two and is not shown to aid clarity.

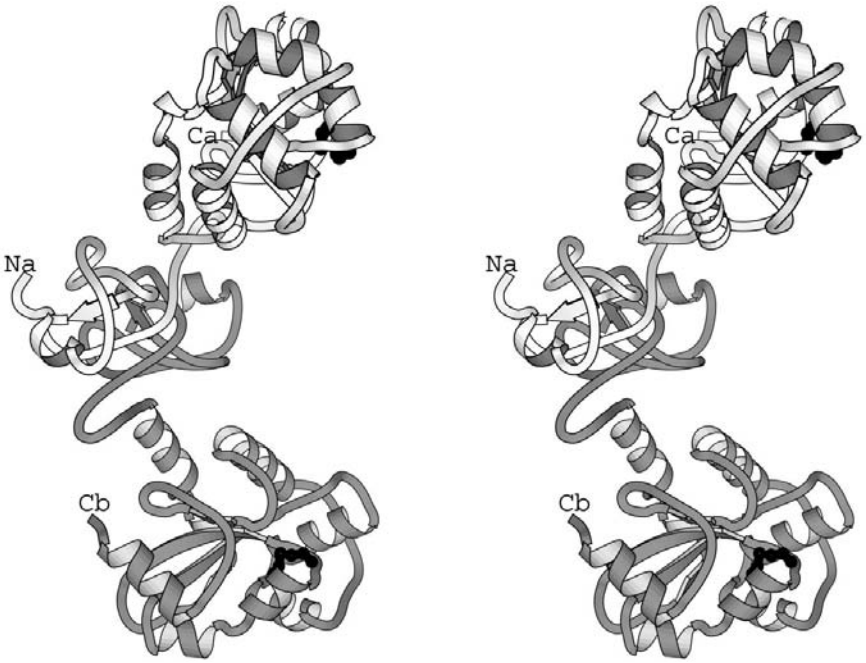

Figure 4
Stereoview of the *H. influenzae* DsbC dimer. The asymmetric unit of the crystal is a monomer, but the molecular symmetry is incorporated into crystallographic symmetry. One monomer is shaded light and the other dark; the termini are labeled for monomers *A* and *B*. The active-site thiol side chains are shown as black spheres. This figure was generated using *BOBSCRIPT* (Esnouf, 1997).

3.3. Comparison of dimerization

Dimerization of DsbC is required for its isomerase and chaperone activity. Purified *H. influenzae* DsbC forms a stable homodimer in solution based on gel-filtration chromatography (unpublished data). Each asymmetric unit contains only one DsbC molecule in the *H. influenzae* crystal. Therefore, the molecular twofold axis is believed to overlap with the crystallographic twofold axis. Similar to *E. coli*

DsbC, the *H. influenzae* DsbC dimer is V-shaped and the N-terminal domain from each monomer forms the dimer interface at the base of the V (Fig. 4). The *H. influenzae* DsbC dimer has a larger angle between the two arms of the V than the *E. coli* DsbC. Dimerization interactions in the *H. influenzae* dimer are similar to those observed with *E. coli* DsbC.

The structure of a covalent complex between *E. coli* DsbC and the DsbD α-domain has been solved recently (Haebel *et al.*, 2002). In it, the S^{γ} atoms of the two active-site Cys98 residues found in the dimer are brought 9 Å closer than was observed in the apo DsbC dimer (from 38 to 29 Å). The conformation of DsbC observed in the complex was referred to as 'closed'. It was suggested that the angle of the central cleft in the DsbC dimer can adjust to the conformation of molecules bound, which would allow DsbC to bind a variety of protein substrates.

Our apo *H. influenzae* DsbC structure suggests that apo DsbC can exist in an even more open conformation, with a distance of 53 Å between the Cys98 in the active sites on the two monomers (Fig. 4). The angle formed between one Cys98 S^{γ} atom, the center of mass of the N-terminal dimer and the other Cys98 S^{γ} atom is 91° in the very open conformation of *H. influenzae* DsbC. By comparison, the angles of the V for the previously observed 'open' and 'closed' conformations are 65 and 55°, respectively. Together with the apo *E. coli* DsbC and *E. coli* DsbC–DsbDα complex structures, the apo *H. influenzae* DsbC structure shows that DsbC dimers can assume a wide range of hinged conformations. Such a property would allow DsbC, as a protein chaperone, to accommodate a broad range of protein substrates. Once bound to this substrate, the two arms in the V-shaped DsbC dimer close to bring the substrate disulfides close to the DsbC active sites to facilitate protein disulfide isomerization or reduction.

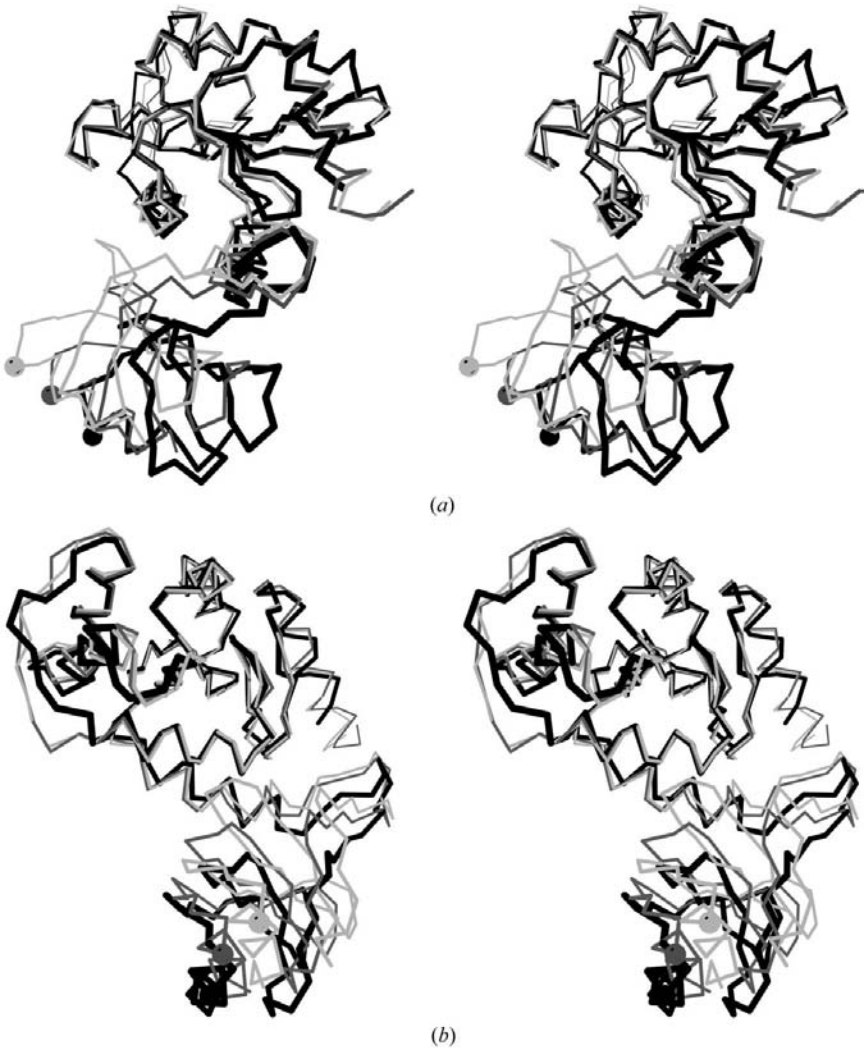

Figure 5
The structural basis for anisotropy in the *H. influenzae* DsbC crystals. Comparison of the enzyme with two forms of *E. coli* DsbC show that the hinge motion of the protein is confined to the *ab* plane. (*a*) A view down the *c* axis, superimposing the C-terminal domains; packing constraints immobilize this domain in *H. influenzae* crystals. The *H. influenzae* protein is shown in black, the apo *E. coli* enzyme in dark gray and the complexed form of *E. coli* in light gray. (*b*) A view normal to the *c* axis in which all three proteins lie in the same plane. This figure was generated using *BOBSCRIPT* (Esnouf, 1997).

3.4. Hinge motion and anisotropy

As mentioned above, the diffraction data for *H. influenzae* DsbC is very anisotropic and in particular is weak in the *ab* plane. Also, the average atomic temperature factor for the N-terminal domain is significantly higher than that for the C-terminal domain and hinge-linker region (99 compared with 76 $Å^2$), indicative of greater thermal motion in the N-terminal domain. This greater thermal motion is likely to be the cause of the reduced number of observed side chains in the N-terminal domain.

Differences in crystal packing between the two domains, together with the inherent mobility of the hinge region, appear to account for the difference in thermal motion and the data anisotropy. The C-terminal domain has crystal-packing contacts on three different sides with symmetry-related C-terminal domains, 'locking' it into position; in contrast, the only crystal-packing contacts for the N-terminal domain are those involved in the formation of the biological dimer. Thus, while the C-terminal domains of the dimer are 'locked' in position, the dimer of N-terminal domains is free to move from the two hinges away from the twofold contact. The propensity of DsbC to move in this way is illustrated in Fig. 5. In Fig. 5(*a*), the *H. influenzae* protein is viewed down the crystallographic *c* axis. The C-terminal domain is superimposed with the C-terminal domains of the *E. coli* enzyme in both its apo form and complexed with the DsbD

α-domain. Note that the N-terminal domains form a sweeping motion in the *ab* plane. The C^{α} position of residue 11 is shown as a marker in each structure as an enlarged sphere. In these three structures, it moves 12.2 Å in the *ab* plane. In Fig. 5(*b*), the view is normal to *c* and the three structures all lie roughly in one plane; the marker C^{α} atom moves only 5.0 Å along the *c* axis. That is, all the hinge motion in DsbC lies essentially in the *ab* plane of the *H. influenzae* crystal. The molecular freedom to move in this direction, coupled with the lack of packing constraints, allows the N-terminal domain to assume a range of thermal motions that is probably manifested as high temperature factors and data anisotropy in the *ab* plane.

4. Conclusion

The structure of *H. influenzae* DsbC at a nominal resolution of 3.3 Å was solved by molecular replacement. The current model shows that *H. influenzae* DsbC has a similar structure to *E. coli* DsbC, although the *H. influenzae* DsbC dimer assumes a more open conformation. This class of enzymes has a structural flexibility that is appropriate to its function of interaction with a wide range of misfolded proteins in order to facilitate disulfide-bond isomerization.

We thank Dr J. J. G. Tesmer for data collection on ALS beamline 8.2.1 (Lawrence Berkeley National Laboratory). This work was supported by NIH grant GM 63593, by the Robert A. Welch Foundation and by the College of Natural Sciences support to the Center for Structural Biology. The Advanced Light Source is supported by the Director, Office of Science, Office of Basic Energy Sciences, Materials Sciences Division, US Department of Energy under contract No. DE-AC03-76SF00098 at Lawrence Berkeley National Laboratory.

References

Bader, M., Hiniker, A., Regeimbal, J., Goldstone, D., Haebel, P. W., Riemer, J., Metcalf, P. & Bardwell, J. C. (2001). *EMBO J.* **20**, 1555–1562.

Bader, M., Muse, W., Ballou, D. P., Gassner, C. & Bardwell, J. C. (1999). *Cell*, **98**, 217–227.

Bardwell, J. C., Lee, J. O., Jander, G., Martin, N., Belin, D. & Beckwith, J. (1993). *Proc. Natl. Acad. Sci. USA*, **90**, 1038–1042.

Bardwell, J. C., McGovern, K. & Beckwith, J. (1991). *Cell*, **67**, 581–589.

Bessette, P. H., Cotto, J. J., Gilbert, H. F. & Georgiou, G. (1999). *J. Biol. Chem.* **274**, 7784–7792.

Brünger, A. T., Adams, P. D., Clore, G. M., DeLano, W. L., Gros, P., Grosse-Kunstleve, R. W., Jiang, J.-S., Kuszewski, J., Nilges, N., Pannu, N. S., Read, R. J., Rice, L. M., Simonson, T. & Warren, G. L. (1998). *Acta Cryst.* D**54**, 905–921.

Chen, J., Song, J. L., Zhang, S., Wang, Y., Cui, D. F. & Wang, C. C. (1999). *J. Biol. Chem.* **274**, 19601–19605.

Collaborative Computational Project, Number 4 (1994). *Acta Cryst.* D**50**, 760–763.

Collet, J. F., Riemer, J., Bader, M. W. & Bardwell, J. C. (2002). *J. Biol. Chem.* **277**, 26886–26892.

Edeling, M. A., Guddat, L. W., Fabianek, R. A., Thony-Meyer, L. & Martin, J. L. (2002). *Structure*, **10**, 973–979.

Esnouf, R. M. (1997). *J. Mol. Graph.* **15**, 132–134.

French, S. & Wilson, K. (1978). *Acta Cryst.* A**34**, 517–525.

Guilhot, C., Jander, G., Martin, N. L. & Beckwith, J. (1995). *Proc. Natl Acad. Sci. USA*, **92**, 9895–9899.

Haebel, P. W., Goldstone, D., Katzen, F., Beckwith, J. & Metcalf, P. (2002). *EMBO J.* **21**, 4774–4784.

Jones, T. A., Zou, J.-Y., Cowan, S. W. & Kjeldgaard, M. (1991). *Acta Cryst.* A**47**, 110–119.

Kim, J. H., Kim, S. J., Jeong, D. G., Son, J. H. & Ryu, S. E. (2003). *FEBS Lett.* **543**, 164–169.

Kishigami, S., Kanaya, E., Kikuchi, M. & Ito, K. (1995). *J. Biol. Chem.* **270**, 17072–17074.

Kissinger, C. R., Gehlhaar, D. K., Smith, B. A. & Bouzida, D. (2001). *Acta Cryst.* D**57**, 1474–1479.

Kurokawa, Y., Yanagi, H. & Yura, T. (2003). *J. Biol. Chem.* **276**, 14393–14399.

Laskowski, R. A., MacArthur, M. W., Moss, D. S. & Thornton, J. M. (1993). *J. Appl. Cryst.* **26**, 283–291.

Lodowski, D. T., Pitcher, J. A., Capel, W. D., Lefkowitz, R. J. & Tesmer, J. J. G. (2003). *Science*, **300**, 1256–1262.

McCarthy, A. A., Haebel, P. W., Torronen, A., Rybin, V., Baker, E. N. & Metcalf, P. (2000). *Nature Struct. Biol.* **7**, 196–199.

Martin, J. L., Bardwell, J. C. & Kuriyan, J. (1993). *Nature (London)*, **365**, 464–468.

Maskos, K., Huber-Wunderlich, M. & Glockshuber, R. (2003). *J. Mol. Biol.* **325**, 495–513.

Otwinowski, Z. & Minor, W. (1997). *Methods Enzymol.* **276**, 307–326.

Qiu, J., Swartz, J. R. & Georgiou, G. (1998). *Appl. Environ. Microbiol.* **64**, 4891–4896.

Raina, S. & Missiakas, D. (1997). *Annu. Rev. Microbiol.* **51**, 179–202.

Read, R. J. (1986). *Acta Cryst.* A**42**, 140–149.

Rietsch, A., Belin, D., Martin, N. & Beckwith, J. (1996). *Proc. Natl Acad. Sci. USA*, **93**, 13048–13053.

Rietsch, A., Bessette, P., Georgiou, G. & Beckwith, J. (1997). *J. Bacteriol.* **179**, 6602–6608.

Zapun, A., Missiakas, D., Raina, S. & Creighton, T. E. (1995). *Biochemistry*, **34**, 5075–5089.